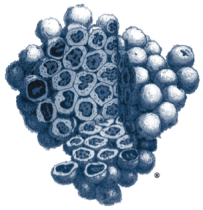

STEM CELLS®

Persistent dopamine functions of neurons derived from embryonic stem cells in a rodent model of Parkinson's disease

Jose A. Rodríguez-Gómez, Jian-Qiang Lu, Iván Velasco, Seth Rivera, Sami S. Zoghbi, Jeih-San Liow, John L. Musachio, Frederick T. Chin, Hiroshi Toyama, Jurgen Seidel, Michael V. Green, Panayotis K. Thanos, Masanori Ichise, Victor W. Pike, Robert B. Innis and Ron D.G. McKay

Stem Cells published online Dec 14, 2006;
DOI: 10.1634/stemcells.2006-0386

Stem Cells Express, published online December 14, 2006; doi:10.1634/stemcells.2006-0386

Embryonic Stem Cells

Persistent dopamine functions of neurons derived from embryonic stem cells in a rodent model of Parkinson's disease.

Running title: Function of ES cell grafts in Parkinsonian rats

Jose A. Rodríguez-Gómez*[1,6], Jian-Qiang Lu*[2,7], Iván Velasco[1,8], Seth Rivera[4], Sami S. Zoghbi[2], Jeih-San Liow[2], John L. Musachio[2], Frederick T. Chin[2], Hiroshi Toyama[2], Jurgen Seidel[3], Michael V. Green[3], Panayotis K. Thanos[4,5], Masanori Ichise[2], Victor W. Pike[2], Robert B. Innis†[2], Ron D.G. McKay†[1]

[1]*Laboratory of Molecular Biology, NINDS Porter Neuroscience Research Center;* [2]*Molecular Imaging Branch, NIMH;* [3]*Clinical Center, National Institutes of Health, Bethesda, MD 20892;* [4]*Medical Department, Brookhaven National Laboratory, Upton, New York 11973-5000;* [5]*Laboratory of Neuroimaging, National Institute on Alcohol Abuse and Alcoholism, National Institutes of Health, Bethesda, MD 20892.*

Current addresses: [6]*Laboratorio de Investigaciones Biomédicas, Hospital Universitario Virgen del Rocío, Seville, 41013, Spain;* [7]*Department of Pathology & Lab Medicine, Foothills Medical Centre, Calgary, AB T2N 2T9. Canada*; [8]*Instituto de Fisiología Celular, Universidad Nacional Autónoma de México, Mexico City 04510, Mexico.*

**, †Contributed equally to this work as first* or last† authors.*

Received on June 26, 2006; accepted for publication on December 5, 2006.
 1066-5099 doi: 10.1634/stemcells.2006-0386

Correspondence should be addressed to Ron D. G. McKay, Laboratory of Molecular Biology, National Institute of Neurological Disorders and Stroke, 35 Convent Drive, Building 35, Room 3A-201, MSC 3703. Bethesda, MD 20892. E-mail: mckayr@ninds.nih.gov
Six figures and one table.

Key words: Parkinson's disease, embryonic stem cell, transplantation, microdialysis, positron emission tomography, dopamine transporter

Abstract

The derivation of dopamine neurons is one of the best examples of the clinical potential of embryonic stem (ES) cells but the long-term function of the grafted neurons has not been established. Here we show that after transplantation into an animal model, neurons derived from mouse ES cells survived for over 32 weeks, maintained midbrain markers and had sustained behavioral effects. Microdialysis in grafted animals showed DA release was induced by depolarization and pharmacological stimulants. Positron emission tomography (PET) measured the expression of pre-synaptic dopamine transporters (DAT) in the graft and also showed that the number of postsynaptic DA D_2 receptors was normalized in the host striatum. These data suggest that ES-cell derived neurons show DA release, reuptake and stimulate appropriate post-synaptic responses for long periods after implantation. This work supports continued interest in ES cells as a source of functional DA neurons.

Introduction

Parkinson's disease is a neurodegenerative disorder characterized by the progressive loss of dopaminergic neurons in the substantia nigra. Transplantation of dopamine (DA) neuron precursors into the striatum of patients suggests that neuronal replacement may be a feasible treatment [1]. However, two recent double-blind transplantation trials with Parkinson's disease patients raise concerns about both the therapeutic benefit and disabling consequences of fetal cell grafting [2, 3, 4]. Further development of a transplantation therapy requires a consistent source of DA neurons and clear evidence of DA function in pre-clinical models.

Fetal human tissue is currently used as a source of DA neurons, but this supply is limited and difficult to develop as a routine technology. In principle, the controlled proliferation and differentiation of fetal precursor cells is an attractive source for cell-based therapies. Precursor cells in the fetal midbrain can expand in tissue culture and generate DA neurons that provide behavioral recovery in Parkinsonian animals [5, 6]. However, these cells only proliferate for short periods in culture and do not provide sufficient numbers of DA neurons. Embryonic stem (ES) cells may overcome the limitations of fetal donor tissue by offering both extensive cell proliferation and controlled differentiation to DA neurons [7, 8]. DA neurons derived from mouse and non-human primate ES cells integrate and provide behavioral recovery in several experimental animal models [9, 10, 11, 12, 13, 14]. More recent work shows that human ES cells also differentiate into DA neurons, but the function of these cells has not been fully established [15, 16, 17, 18, 19, 20]. Indeed, little evidence exists that neurons derived from ES cells from any species survive with DA function for long periods after grafting to the adult brain.

In the present study, the stability of DA neurons derived from ES cells was analyzed *in vivo* with a particular focus on their dopaminergic properties. Microdialysis was used to directly measure DA and DA breakdown products generated by grafted cells. Positron emission tomography (PET) imaging was used to measure both the presynaptic dopamine transporter (DAT) and the postsynaptic D_2 dopamine receptor. We found that neurons derived from mouse ES cells survive *in vivo* for several months, express presynaptic dopaminergic features and influence postsynaptic DA response mechanisms in striatal host cells.

Materials and Methods

In vitro differentiation of ES cells to DA neurons. Mouse R1 ES cells were induced to differentiate into neurons with DA phenotype using a previously established five-stage protocol [8]. This method is based on the formation of embryoid bodies (EBs) and further selection, proliferation and differentiation of neural progenitors into postmitotic neurons.

Immunocytochemistry and histological procedures. Cultured cells were fixed for immunostaining either at the proliferation or differentiation stages in 4% paraformaldehyde/0.15% picric acid/phosphate buffered saline (PBS). The analysis of transplanted animals was made essentially as described [10]. Briefly, 32 weeks after grating, rats were anesthetized with sodium pentobarbital and transcardially perfused with isotonic saline, followed by the fixative solution used for cultured cells. The brains were dissected, postfixed for 4 h, cryoprotected with 30% sucrose for 24 - 48 h, and then frozen in isopentane cooled by solid CO_2. Cryostat sections (25 μm) were stained as floating slices. Fixed cells or brain slices were incubated with the primary antibodies overnight at 4 ºC. The following antibodies were used: mouse anti-engrailed-1 (En-1) 1:10 (Developmental Studies Hybridoma Bank, Iowa City, IA); rabbit anti-Lmx1b, 1:5000 (gift from C. Birchmeier); goat anti-Foxa2, 1:50 (Santa Cruz Biotechnology, Santa Cruz, CA); rabbit anti-tyrosine hydroxylase (TH), 1:400 (PelFreeze Biologicals, Rogers, AR); mouse anti-TH, 1:1000 (Sigma); mouse anti-Hu 1:50 (Molecular Probes, Eugene, OR); rabbit anti-Ptx3, 1:1000 (gift from J. P. Burbach); rabbit anti-RALDH1, 1:100 (gift from G. Duester); mouse anti-calbindin, 1:3000 (Sigma) and rat anti-DA transporter (DAT), 1:5000 (Chemicon**,** Temecula, CA). Appropriate fluorescent-tagged secondary antibodies (Molecular Probes) and 4'-6-diamidino-2-phenylindole (DAPI)

nuclear counterstain were used for visualization. We used a Zeiss 510 confocal microscope to make optical sections of the cells after staining. Cells were counted *in vitro* by systematic sampling of 20 X fields. Twenty fields were counted per tissue culture well and 4 wells were analyzed for each condition in three independent differentiation experiments. TH+ somata in grafted animals were counted in every third section on 20 X fields (n=5). Only clearly stained cells with visible dendrites were scored as positive neurons.

Grafting and implantation of microdialysis probe holders. All experimental procedures conformed to the Guide for Care and Use of Laboratory Animals and were approved by the NINDS Animal Care and Use Committee. Taconic Farms (Germanton, NY) provided adult female Sprage-Dawley rats (170-190 g) with unilateral 6-hydroxy-dopamine (6-OHDA) lesions. A total of 8 µg 6-OHDA was infused in 4 µL over 4 min into the nigrostriatal pathway. The animals were housed in a temperature-controlled environment with a 12-h light-dark cycle for at least one week before the experiments began. Standard rat chow and distilled water were supplied *ad libitum*. ES cell-derived neurons were trypsinized at day 2-3 of differentiation stage and re-suspended at 80,000 viable cells per µL after vital trypan blue exclusion counting. Animals were anesthetized with isofluorane, and two grafts were implanted by injecting 3 µL of the cell suspension into the lesioned striatum at the following coordinates: anteroposterior (AP) = + 0.3 mm (first graft), - 0.3 mm (second graft), mediolateral (ML) = -3.0 mm and dorsoventral (DV) = - 6.0 mm relative to bregma and the skull, with the tooth bar set at 0.0 mm. We deposited 0.5 µL of cell suspension (grafted) or medium without cells (sham), waited 1 min, advanced the syringe 0.5 mm dorsally, and injected 0.5 µL. This procedure was repeated 5 times to deposit cells over a distance of 2.5 mm in the

dorsoventral axis. Implanted cells totalled 480,000 per animal – i.e., a number that we previously showed to promote behavioral recovery [10]. We then implanted microdialysis probe holders bilaterally with stereotaxic coordinates AP = 0.0 mm, LM = ± 3.0 mm, and DV = – 2.0 mm and secured them with acrylic cement. Small screws were introduced into the skull, taking care of not damaging the brain, to provide support to the cement, which covered the probe holders and closed the wound completely. Sham and grafted subjects were immunosuppressed with cyclosporine A during the length of the experiment (Neoral, Novartis, 10 mg/kg/day, intraperitoneally, i.p.), starting 24 h before grafting [10].

Rotational behavior. Stereotypic rotational behavior was assessed (Rota Count-8, Columbus Instruments, Columbus, OH) for 70 min after injection of amphetamine (2.5 mg/kg, subcutaneous; Sigma). Asymmetry scores are expressed as net 360º turns per min. Rotations were measured before and after cell grafting. Animals with stable scores of >6 ipsilateral turns per min after lesion were used further. Spontaneous rotational test was performed as described [21].

Microdialysis experiments. Twelve weeks after implantation surgery, 4-mm long microdialysis probes (CMA, Solna, Sweden) were introduced in both striata to measure extracellular monoamine concentrations. *In vitro* recovery experiments with the dialysis membranes had values of 18%, 15%, 17% and 11% for DA, DOPAC, HVA and 5-HIAA, respectively. The probes were perfused with artificial cerebrospinal fluid at 2 µL/min, and fractions were collected every 10 min. Monoamines were stabilized by adding a solution containing 0.1 N perchloric acid, 0.02% EDTA and 1% ethanol, kept at 4 ºC, frozen in dry ice, and then stored at -80 ºC until measurement. Extracellular DA

increases were obtained through chemical depolarization (isosmotic solution with 100 mM potassium chloride), DA uptake blockade (50 μM nomifensine), and reversal of DA uptake (30 μM amphetamine). Dialysate samples were quantified for monoamine content by high-performance liquid chromatography (HPLC) with electrochemical detection (GBC, Hubbardston, MA). No recovery correction was performed.

[^{18}F]FECNT Imaging. PET DAT scans were performed at NIH 24 - 28 weeks following ES-cell transplantation. Animals were anesthetized with 1.5-2.0 % isoflurane, and body temperature was maintained at 36.5 - 37.0 ºC. The ATLAS (Advanced Technology Laboratory Animal Scanner) PET device has an aperture of 11.8 cm diameter and a 2 cm axial field-of-view [22]. Each animal was positioned prone in the PET scanner so that striatum and cerebellum were within the field of view. Images were reconstructed by 3D ordered subset expectation maximization algorithm (3 iterations), achieving a 1.65 mm full-width at half maximum resolution at the center [23, 24, 25]. The reconstructed voxel size was 0.56 x 0.56 x 1.125 mm. Coronal images were created for subsequent data analysis. Image data were not corrected for attenuation or scatter, which was relatively minor because of the rat's small head.

[^{18}F]FECNT was prepared as previously described [26, 27] with the principal modification being that the intermediate 1-[^{18}F]fluoro-2-tosyloxyethane was purified by semi-preparative HPLC (acetonitrile/water gradient; Waters RP18 XTerra column 7.8 mm x 300 mm) and isolated in acetonitrile via solid phase extraction. The ^{18}F-labeled alkylating agent was then reacted with 0.75 mg of CNT (2ß-carbomethoxy-3-ß-(4-chlorophenyl)nortropane. The alkylation reaction was performed in an open, heated vessel (110 °C; 10 min), and the acetonitrile solvent (originally ~1.2 mL) was

concentrated to less than 0.1 mL by a low flow of helium gas (10 mL/min) that was bubbled into the solution. A second HPLC purification on the semi-preparative column using an acetonitrile/10 mM NH_3 gradient afforded [^{18}F]FECNT of high chemical and radiochemical purity. Specific activity at the time of injection ranged from 42.6 GBq/μmol (1.2 Ci/μmol) to 235.6 GBq/μmol (6.4 Ci/μmol), with a mean ± S.D. of 126.5 ± 75.7 GBq/μmol (3.4 ± 2.0 Ci/μmol).

To establish the methodology with [^{18}F]FECNT, we used three groups of naïve rats that underwent one of the following procedures: (1) Five animals received a bolus injection of 15-34 MBq/h [^{18}F]FECNT and were scanned for 120 ~ 180 min using 24 or 27 frames of increasing duration (6 x 20 s, 5 x 1 min, 4 x 2 min, 3 x 5 min, 3 x 10 min, 3-6 x 20 min). (2) Five animals received 32-63 MBq/h [^{18}F]FECNT as a constant infusion for 240 min (30 frames: 6 x 20 s, 5 x 1 min, 4 x 2 min, 3 x 5 min, 3 x 10 min, 9 x 20 min), during which serial blood samples (25 μL) were collected every 20 min via a femoral artery catheter. (3) Four animals were injected subcutaneously with methylphenidate (10 mg/kg) at the midpoint of constant infusion that was the junction of two 100-min acquisition (46 frames: 6 x 20 s, 5 x 1 min, 4 x 2 min, 3 x 5 min, 3 x 10 min, 2 x 20 min and 6 x 20 s, 5 x 1 min, 4 x 2 min, 3 x 5 min, 3 x 10 min, 2 x 20 min).

For 6-OHDA-lesioned rats, [^{18}F]FECNT was administered as a constant infusion of 26 - 37 MBq/h and a volume of 0.45 - 0.75 mL/h. Rats with 6-OHDA lesions were uniformly scanned for 240 min, and a blood sample (50 μL) was collected from a lateral saphenous vein between 180 and 190 min after starting the infusion. Blood samples were centrifuged at 1,800 *g* for 3 min. Plasma samples (50 - 80 μL) were mixed with 300 μL of acetonitrile containing UV-standard of FECNT followed by the addition of

100 μL of distilled water and mixed well. Radioactivity in this mixture was measured to calculate the concentration of total radioactivity (i.e., parent tracer plus metabolites) in plasma. Deproteinized plasma samples were then centrifuged at 9,400 *g* for 4 min to remove the denatured proteins. To correct plasma parent concentrations for the presence of radiometabolites, the supernatant was analyzed with reversed phase HPLC on Novapak C_{18} column (Waters Corp., Milford, MA) with a radial compression module RCM-100 and a mobile phase of MeOH:H_2O:Et_3N (80:19.9:0.1) at a flow rate of 1.5 mL/min. Recovery was always more than 90 %. All radioactivity measurements were decay-corrected to the time of injection ($T_{1/2}$ = 110 min). We found that the concentrations of parent [^{18}F]FECNT in plasma were similar in femoral arterial and saphenous venous samples (unpublished data).

We recently reported that a radiolabeled metabolite of [^{18}F]FECNT accumulates in rat brain and confounds the ability to quantify DAT [28]. The radiometabolite results from N-dealkylation and is an ^{18}F-labeled two-carbon fragment, which rapidly converts from fluoroethanol to fluoroacetyladhyde to fluoroacetic acid. The latter is charged and accumulates in brain. As described in Results, we developed a method of constant infusion of [^{18}F]FECNT for the current study to provide reliable quantitation of the density of DAT in rodent brain. In brief, after constant infusion of the radiotracer, the concentration of parent radiotracer in plasma as well as specific binding in brain (defined as activity in striatum minus that in cerebellum) becomes stable. The ratio of specific binding in brain to the plasma radiotracer concentration is distribution volume, which is proportional to density (Bmax) of DAT [29].

[^{11}C]Raclopride Imaging. After DAT imaging at NIH, the animals were transported to Brookhaven National Laboratory for PET DA D_2 receptor scans that were performed 30 – 32 weeks after ES-cell transplantation. Rats were anesthetized intraperitoneally with ketamine (100 mg/kg) / xylazine (10 mg/kg) and placed in a stereotaxic head holder in a prone position on the Concorde microPET R4 scanner bed (Concorde Microsystems, Knoxville, TN). Animals were then injected via tail vein catheter with a mean dose of 1.56 nmol/kg [^{11}C]raclopride (6.5 ± 3.0 MBq for grafted and 5.5 ± 2.8 MBq for sham; specific radioactivity was 81 – 170 GBq/μmol and injected volumes were <500 μL). [^{11}C]raclopride binding in the microPET R4 has been previously demonstrated as a reproducible and suitable method to study the D_2 receptor availability in the rodent brain [30, 31]. The microPET R4 scanner has a 12-cm animal port with an image field of view of ~11.5 cm. Total acquisition time was 60 min (24 frames: 6 x 10 s, 3 x 20 s, 8 x 1 min, 4 x 5 min, 3 x 10 min), and data acquired in fully dimensional mode with maximum axial acceptance angle (± 28 deg). Images were reconstructed using FORE rebinning [32], followed by 2-dimensional filtered back-projection with a ramp cutoff at Nyquist frequency. Using the rat stereotaxic atlas [33] and the Hardarian glands as reference points, the coronal planes of the striatum and cerebellum were identified as slices 6 and 16, respectively, caudal to the Hardarian glands (slice thickness 1.2 mm) [34, 32, 33, 30].

Image Analysis. To define brain anatomic structures, MRI images were acquired using a 7T horizontal small animal MRI system (Bruker Biospin, Billerica, MA) with a spin echo sequence (TR = 1500 ms, TE = 10.29 ms) from naïve rats with a similar body weight. PET images were analyzed with PMOD v2.4 (pixel-wise modeling computer software, PMOD Group, Zurich, Switzerland). Coregistration (FSL Library, Oxford) of

PET with the MRI images facilitated the placement of regions of interest over striatum and cerebellum. In the images of both [^{18}F]FECNT and [^{11}C]raclopride, the right striatum (non-lesioned side) was typically delineated on 3-4 different coronal planes, from which a central single image plane was chosen for analyzing regions of interest so as to minimize axial partial-volume effects [31]. The regions of interest (~22-28 mm^3) followed the anatomical contour of the right striatum in the MR image (Fig. 5D) and/or the stereotaxic rat brain atlas [33]. To be symmetrical, each template of the right striatum was copied and pasted/mirrored to the left striatum, with slight manual adjustment of placement according to anatomical references.

DAT binding of [^{18}F]FECNT was quantified as an equilibrium distribution volume that was calculated as the stable level of specific binding in the brain divided by the stable plasma concentration of radiotracer [35, 29]. Specific binding was defined as the uptake in striatum minus that in cerebellum. D_2 receptor binding of [^{11}C]raclopride was analyzed with a multilinear reference tissue model [25].

Statistical analysis. Each group of data passed a normality test before it was analyzed with parametric statistics. An unpaired two-tailed student's *t*-test was used to assess group differences; a paired two-tailed student's *t*-test was performed to make comparisons between bilateral striata. Significance was considered when $p < 0.05$ or $p < 0.01$.

Results

Expression of midbrain specific markers in precursors and differentiated neurons.

Mouse ES cells were differentiated following a five-stage protocol that allows efficient differentiation of DA neurons [8, 10]. Markers of regional identity such as En1, Pax2 and Otx2 showed that this method generated proliferating neural precursors with mid- and hindbrain phenotypes. The mid/hindbrain boundary region and the mesencephalic floor plate act as organizing centers regulating neuronal differentiation by the production of fibroblast growth factor (FGF)-8 and sonic hegdehog (Shh) [36]. The differentiation of ES cells into DA precursors was regulated by these signals and, thus, provided additional evidence that the *in vitro* generated cells mimic aspects of normal midbrain development. The five stages of the differentiation protocol are: (1) proliferating ES cells; (2) differentiating ES cell aggregates, EBs; (3) nestin-positive cells that migrate from the EBs under minimal growth conditions; (4) a proliferative step when these CNS precursor cells expand in number in the presence of FGF-8 and Shh; and (5) a differentiation step when neurons are generated. At step 4, many cells expressing the transcription factors En1, Lmx1b and Foxa2 were observed (Fig.1A, B). Approximately 40 % of the total cells expressed En1, a gene that has an important role in midbrain progenitors (Fig. 1B) [37]. 8 % of the cells co-expressed all three genes (Fig. 1B). Cell autonomous expression of Lmx1b and Foxa2 are thought to be essential for the differentiation of DA neurons and the floor plate [38, 39]. During normal development, Foxa2-positive floor plate cells directly generate the Lmx1b-positive DA neurons [40] (Kittappa, Wang and McKay; unpublished observations). The co-expression of Foxa2 and Lmx1b suggests that this precursor cell type is also present in

ES derived En1-positive populations (Fig. 1A, B). The presence of En1+, Foxa2-, Lmx1b+ cells was not expected from *in vivo* studies and might reflect short term regulation of the expression of the Foxa2 protein rather than a cell of a different fate [41]. These data show that 30 % of the cells express En1 in combination with Foxa2 and Lmx1b, genes expressed in the ventral midbrain.

In the final step, this protocol generates neurons from neural precursors. After 10 days of differentiation in stage 5, the gene expression profile of the differentiated neurons was assessed. All tyrosine hydroxylase positive (TH+) cells expressed the neuronal marker Hu (Fig. 1C). Approximately 11 ± 1 % of Hu+ cells were also TH+. This result is consistent with previous data suggesting that without genetic manipulation a small proportion of neurons acquire the dopaminergic fate [8,10]. Foxa2 is also expressed in mature DA neurons (Kittappa, Wang and McKay; unpublished data) and 30 ± 3 % of the Foxa2+ neurons generated *in vitro* co-expressed TH (Fig. 1C). En1 was co-expressed in all TH+ neurons, as has been observed in differentiated adult DA neurons and in DA neurons generated in the lab (Fig. 1C) [37, 10]. Ptx3 is a transcription factor specifically expressed in DA neurons [42]. Ptx3 was co-expressed in the great majority of TH+ neurons (99 ± 1 %; Fig. 1C). Calbindin is expressed in the dorsal part of the substantia nigra *pars compacta* and the ventral tegmental area of rats [43]. Only a small proportion (1 ± 0.1 %) of the TH+ neurons co-expressed calbindin *in vitro* (Fig. 1C). RALDH1 is also a specific marker of DA neurons in the ventral part of the substantia nigra *pars compacta* [44, 45]. In ES cells-derived neurons, 42 ± 1 % of TH+ cells express RALDH1 (Fig. 1C). The DAT is critical to appropriate neurotransmitter recycling [46, 47]. DAT was expressed by TH+ cells after longer times of *in vitro* differentiation (20 days in stage 5, Fig. 1C). Calretinin expression is

found in the substantia nigra *pars compacta* and the ventral tegmental area. Calretinin+ cells were observed in stage 5, but none of them co-expressed TH (data not shown). These data suggest that TH+ neurons derived from ES cells have patterns of gene expression characteristic of dopaminergic cells in the ventral midbrain.

In this study the mouse ES cells were not genetically manipulated and simple differentiation conditions for DA neurons were employed. The presence of neurons co-expressing TH and other markers of the ventral DA cell in the substantia nigra suggests that ES cells may generate the DA neuron type at most risk in Parkinson's disease [48]. Other types of neurons are also present. A clear example is the small proportion of serotonin+ neurons that may represent hindbrain monoaminergic cells as we have previously noted [10]. This analysis of gene expression raised the question of whether the transplanted population of cells had sufficient DA neurons of the ventral *pars compacta* type to be effective in the lesioned striatum.

Long-term sustained behavioral recovery induced by partial restoration of DA striatal terminal field.

Neurons derived from the same batch as characterized above were grafted into the striatum of 6-OHDA lesioned animals. The behavior of transplanted animals was measured for up to 32 weeks after the surgery as a first measure of long-term survival of functional grafted neurons. Four weeks after implantation into the dorsal striatum, the grafts caused an abrupt change of amphetamine-induced rotational behavior (Fig. 2A). The kinetics of the behavioral recovery was comparable to that in our previous study [10]. In contrast, a gradual change in behavior has been reported when no specific *in*

vitro steps were used to control ES cell differentiation prior to grafting [9]. With the exception of a slight change at 12 weeks after grafting that is coincident with the placement of a microdialysis probe and a possible disruption of dopaminergic terminals, this behavioral change was stable for 32 weeks. Non-pharmacological evaluation of rotational behavior was also performed until 14 weeks after transplantation demonstrating significant recovery (Fig. S1).

ES cell-derived progeny in the host brains were identified with the mouse-specific M2 antibody, allowing clear identification of the graft (Fig. 2B). TH+ cells with elaborate dendritic processes were observed. The maintenance of the midbrain phenotype in grafted TH+ neurons was assessed by the expression of some midbrain-related markers. Grafted TH+ neurons expressed RALDH1 and calbindin (Fig. 2B). Differently from the *in vitro* situation, we found that some TH+ neurons in the graft expressed calretinin (Fig. 2B). The grafts projected a dense extension of TH-positive processes into the dorso-lateral striatum (Fig. $2C_1$). RALDH1 immunostaining identified projections in a similar distribution to TH in the dorsal striatum (Fig. $2C_3$). On the unlesioned side of the brain, RALDH1-positive processes from the DA neurons of the ventral substantia nigra projected to the dorso-lateral striatum, as previously reported (Fig. $2C_4$) [44]. At 32 weeks, 5385 ± 4638 (mean ± S.E.M.) TH+ cells were found in lesioned striatum of grafted animals. Thus, grafted DA neurons survived in large numbers for 32 weeks, maintained midbrain markers, extended strong RALDH1 projection to the dorso-lateral striatum and regulated behavior.

DA release and monoamine levels in grafted animals.

Microdialysis was used to monitor DA production by the grafted cells. Extracellular monoamine levels were measured simultaneously in the lesioned and non-lesioned striata of sham and grafted animals. Baseline DA levels were elevated on both sides of the brain after grafting, although only in the grafted side reached statistical significance when comparison was performed against both striata of sham animals (Table 1). In contrast to DA itself, the metabolites DOPAC and HVA showed right/left asymmetry. Grafting caused a partial restoration of DOPAC and HVA concentrations to about 10 % of basal levels (Table 1). The level of the 5-HT metabolite, 5-HIAA, was not altered by the lesion to the DA neurons. Meanwhile, a significantly higher level was found in the grafted striatum either as a consequence of 5HT-positive neurons in the graft as we have shown [10] or due to sprouting of intrinsic serotonergic afferents to striatum induced by grafted DA cells [49, 50]. The cause and consequence of bilaterally elevated basal DA levels are not known but these data demonstrate that DA and its metabolites are elevated in grafted animals.

Extracellular DA levels were measured following three pharmacological challenges: (1) depolarization induced by K^+ ions, (2) inhibition of DAT reuptake with nomifensine, and (3) administration of amphetamine, which causes the release of DA via DAT [51]. Perfusion of isosmotic 100 mM K^+, 50 μM nomifensine and 30 μM amphetamine each caused increased DA levels in the non-lesioned striata (Fig. 3A). On the lesioned side of sham animals, treatment evoked no change in DA levels establishing that the lesions were virtually complete (Fig. 3B). Although DA levels were much lower than those in non-lesioned sides, the ES cell-derived neurons

responded to the three treatments (Fig. 3B). Significant differences were found between sham and grafted groups after K^+-induced depolarization and nomifensine perfusion. In the case of amphetamine, the differences did not reach statistical significance, perhaps due to the variability of the graft response. In both grafted and non-lesioned sides, DOPAC and HVA values decreased after high potassium and amphetamine stimulation as has been previously shown in grafts of DA neurons derived from fetal midbrain (Fig. 3C) [52]. These measurements show that depolarization and DAT blockade elevates extracellular DA levels.

[^{18}F]FECNT imaging showed partial recovery of DA terminals in the lesioned striatum following transplantation.

PET provides a useful non-invasive measure of PD-related changes associated with disease severity [53, 54]. PET imaging has been used to monitor the function of grafted human fetal DA neurons [55, 2, 56, 57]. We developed a method that was independent of cerebral blood flow to measure the abundance of the pre-synaptic DAT in the striatum of rats, using the recently developed radiotracer, 2β-carbomethoxy-3β-(4-chlorophenyl)-8-(2-fluoroethyl)nortropane([^{18}F]FECNT) [26, 27]. We found that [^{18}F]FECNT generates a radiolabeled two-carbon fragment that accumulates in rat brain [28]. The levels of this radiometabolite were measured following injection of the radiotracer (Fig. 4A). The radioactive signal in the cerebellum was stable after about ~30 min. In contrast, the striatum with a high density of DAT showed a stronger signal that declines as the ligand dissociates from the transporter.

These observations led us to administer [^{18}F]FECNT as a constant infusion to achieve steady state levels of parent radiotracer in plasma and equilibrium levels of receptor binding in brain. Following constant infusion of [^{18}F]FECNT, radioactivity in both striatum and cerebellum increased for at least 240 min, but the substraction (STR-CBL) of these two signals was stable after ~120 min (Fig. 4B). Specific binding was defined as the difference between uptake in striatum and cerebellum. This specific uptake reached equilibrium levels by 150 min. The slopes of the fitted lines were only 5.6 ± 4.6 percent per hour, expressed as the mean ± S.D. of the absolute value of slope relative to the value at 150 min (n = 5 rats). Measurements of arterial blood samples showed plasma [^{18}F]FECNT reached steady-state after ~150 min constant infusion (Fig. 4B). Plasma concentrations of the parent tracer separated from radiometabolites of individual rats after 150 min of constant infusion were fitted linearly. The slopes of these fitted lines were 3.7 ± 5.6 percent per hour, expressed as the mean of the absolute values. Injection of methylphenidate displaced the specifically bound signal in the striatum to background levels providing additional support for the specific measurement of DAT in the striatum (Fig. 4C).

Distribution volume is a time- and blood flow-independent parameter that is linearly proportional to receptor density [35]. The constant infusion paradigm allowed a relatively simple calculation of distribution volume as the mean specific binding (= striatum minus cerebellum) from 150 to 210 min divided by the plasma radiotracer concentration at 180 - 190 min. The non-lesioned side (right) of the striatum preserved robust uptake of the tracer (Fig. 5B), similar to concentrations seen in naive animals (Fig. 5A). In contrast, uptake in the lesioned (left) striatum of sham rats, measured as the ratio of the lesioned/non-lesioned was reduced by more than 90 % (Fig. 5B, E). The

tracer uptake was not significantly different in rats receiving the sham procedures (5 ± 3 %) compared to no-intervention lesioned animals (4 ± 3 %; Fig. 5E). In contrast, tracer uptake was partially restored to 38 ± 17 % of controls in the lesioned striatum after grafting (Fig. 5C, E; $p < 0.01$).

Specific binding of [^{18}F]FECNT in the lesioned and transplanted striatum (Fig. 6B) was higher than that of sham animals (Fig. 6A). The distribution volumes of the non-lesioned striata were similar in sham and transplanted rats (Fig. 6C). In contrast, the distribution volumes of the lesioned striata were significantly increased by transplantation (Fig. 6C; 6.71 ± 1.7 vs. 1.15 ± 0.23, $p < 0.01$; mean ± S.E.M.). Distribution volume measurements correct for potential blood flow changes in the lesioned striata and show that grafting is associated with long-term expression of DAT.

[^{11}C]raclopride imaging indicated normalization of upregulated postsynaptic D_2 receptors.

PET imaging was also performed with [^{11}C]raclopride, which binds to D_2 dopamine receptors that are present postsynaptically on a subset of striatal medium spiny neurons. Treatment with 6-OHDA caused asymmetrical uptake of [^{11}C]raclopride, consistent with increased density of D_2 receptors on the side of the lesion [58]. The binding potential of [^{11}C]raclopride increased significantly in sham animals when left and right striata were compared (2.01 ± 0.28 vs. 1.52 ± 0.34, $p < 0.01$, n=4, mean ± S.E.M.). Transplantation normalized D_2 receptors so that the uptake of [^{11}C]raclopride was similar in both striata (1.51 ± 0.18 vs 1.50 ± 0.08, n=5, mean ± S.E.M.) and significantly different to left side of sham animals (p=0.01; Fig. S2). These data suggest

that grafted neurons act on host targets cells to correct the super-sensitive increase in DA D_2 receptors.

Discussion

To validate ES cells as a suitable source of DA neurons for cell-based therapy in Parkinson's disease, it is important that the neurons maintain DA neurotransmitter functions for prolonged periods. In previous studies we have used electrophysiological and behavioral tools to characterize grafted neurons [10]. However, the electrophysiological approach may be subject to a bias due to the choice of specific neurons for recording and the behavioral measures are indirect tests of neuronal function. In this work we have defined long-term dopamine function in grafted animals. The expression of En1, Lmx1b and Foxa2 characterizes neural progenitor cells generated from ES cells as midbrain cells. After further *in vitro* differentiation, many TH+ neurons maintained the midbrain phenotype defined by expression of En1, Foxa2, Ptx3 and RALDH1. These results extend our previous observations by showing that ES cells without genetic modification, generate neurons that sustain dopamine functions for long periods after grafting.

The ES cell-derived DA neurons restored the terminal axonal field in the dorso-lateral striatum and expressed the midbrain markers calbindin, calretinin and RALDH1 suggesting that a at least a proportion of the grafted TH+ neurons maintain this specific midbrain phenotype following transplantation. Retinoic acid modulates the level of striatal DA receptors [59, 60, 61] and retinoic receptor mutant mice show locomotor defects that can be related to decreased levels of DA receptors [62]. Future work should more fully characterize the DA neurons in the graft to determine if RALDH1-positive cells specifically project to the host and analyze the role of retinoic acid on pre- and post-synaptic functions.

Previous studies show that the effect of grafted primary cells on behavior requires the continued presence of DA neurons [63]. The behavioral data reported here show that transplanted animals have altered behavior for seven months. Microdialysis suggests that the grafted cells have activity-dependent release and a high affinity reuptake system for dopamine. The elevated baseline DA level compared to the partial recovery of stimulated DA release points to autoregulatory mechanisms that maintain a normal DA tone despite the inadequate restoration of dopaminergic synapses. A similar phenomenon has been observed in studies of grafted fetal nigral tissue [64, 65, 66]. A canditate to control baseline DA level is the DAT. PET chemistry confirms the expression of the DAT, however post-translational modifications regulate DAT function and may explain the elevated DA level in the presence of DAT [67, 51].

The PET study supports the utility of DAT imaging as a noninvasive *in vivo* marker for the survival of grafted DA neurons. [^{18}F]FECNT was previously used in monkeys [26], healthy human subjects, and patients with Parkinson's disease [27], with a high ratio of specific to nonspecific uptake. Contrary to prior reports [26], [^{18}F]FECNT showed significant accumulation of a polar radiometabolite in rat brain [28]. Because of the time dependent changes in both parent and radiometabolite in brain following a typical bolus injection, no single time point could be *a priori* selected to measure DAT density. For example, Fig. 4A shows that the ratio of striatum to cerebellum continuously declined after about 30 min. At what time does this ratio of specific to nonspecific uptake reflect DAT density? In the current study, we administered [^{18}F]FECNT as a constant infusion and obtained temporally stable levels of specific binding in striatum as well as the concentration of parent radiotracer in plasma. Distribution volume is the ratio at equilibrium of specific binding in brain to the

concentration of drug in plasma, and it is usually regarded as the "gold standard" measurement of *in vivo* receptor density. A simple left/right ratio of activity in lesioned to non-lesioned striata can be used to measure DAT levels (Fig. 5E). However, this ratio can not distinguish whether the lesion or transplant caused any changes to the control side of the brain. Distribution volume can accomplish this comparison, and we report that DAT densities were the same in non-lesioned striata of sham and transplanted animals.

DAT imaging in rodents has been used to monitor fetal mesencephalic [68] and ES-cell transplantation [9]. The latter study used [^{11}C]CFT, a close chemical analog of [^{18}F]FECNT, and found that at nine weeks after transplantation, the grafted striata of animals with behavioral improvement reached ~75-90 % of DAT levels in the contralateral/non-lesioned side [9]. We report DAT levels of only ~40 % in the graft, with wide variation from ~15 – 55 %. The difference between these two studies may be caused by the development of teratomas in the previous study and altered blood flow. In animals grafted with the multi-step protocol no teratomas were found and this is a pre-requisite for the long survival times studied here. Our results show that significant behavioral recovery occurs when ~40 % of DA terminals are restored.

The level of D_2 receptor expression on striatal neurons was measured by [^{11}C]raclopride PET imaging. Suppression of upregulated postsynaptic D_2 receptors by fetal DA grafts has been shown in Parkinsonian rats [69, 70, 71] and in a PD patient 10 years after fetal transplantation [55]. Our data show that D_2 receptor densities may be normalized throughout the striatum despite the partial restoration of DA fibers found in the grafted animals. Efficient uptake of DA has been shown in primary grafted DA

neurons [65, 72, 73] but other studies report diffusion of extracellular DA that may elevate DA tone over non-reinnervated areas [74, 75, 76]. The elevated baseline DA we report in grafted animals may account for the normalization of D_2 receptor binding. Recent work shows that DA denervation leads to rapid changes in spine density in striato-pallidal medium spiny neurons [77]. It will be interesting to analyze other features of postsynaptic neurons including spine density in grafted animals.

In summary, the data presented here show that both pre- and postsynaptic functions can be restored by grafting DA neurons derived from ES cells. The immortal nature of ES cells will allow genetic manipulations to more precisely define the mechanisms regulating the survival and function of DA neurons. This feature will be particularly valuable for cell-therapy studies with human ES cells.

ACKNOWLEDGEMENTS: We thank Drs. Raja Kittappa and Sachiko Murase for valuable advice and discussion and Jeeva Munasinghe (NINDS) for his technical help with acquiring rat MRI images. We are grateful to Carmen Birchmeier (Max-Delbruck-Center of Molecular Medicine, Berlin, Germany), J. Peter Burbach (Rudolph Magnus Institute of Neuroscience, Utrech, The Netherlands) and Greg Duester (Burnham Institute, La Jolla, California), for their gifts of antibodies. I.V. was a Pew Latin American Fellow during his stay at NIH and had partial support from DGAPA, UNAM (IN226703). This work was supported in part by the Intramural Program of NIMH (project Z01-MH-002795-04).

REFERENCES

1. Lindvall O, Bjorklund A. Cell therapy in Parkinson's disease. NeuroRx. Oct 2004;1(4):382-393.

2. Freed CR, Greene PE, Breeze RE, et al. Transplantation of embryonic dopamine neurons for severe Parkinson's disease. N Engl J Med. Mar 8 2001;344(10):710-719.

3. Olanow CW, Goetz CG, Kordower JH, et al. A double-blind controlled trial of bilateral fetal nigral transplantation in Parkinson's disease. Ann Neurol. Sep 2003;54(3):403-414.

4. Hagell P, Piccini P, Bjorklund A, et al. Dyskinesias following neural transplantation in Parkinson's disease. Nat Neurosci. Jul 2002;5(7):627-628.

5. Studer L, Tabar V, McKay RD. Transplantation of expanded mesencephalic precursors leads to recovery in parkinsonian rats. Nat Neurosci. Aug 1998;1(4):290-295.

6. Sanchez-Pernaute R, Studer L, Bankiewicz KS et al. In vitro generation and transplantation of precursor-derived human dopamine neurons. J Neurosci Res. Aug 15 2001;65(4):284-288.

7. Kawasaki H, Mizuseki K, Nishikawa S, et al. Induction of midbrain dopaminergic neurons from ES cells by stromal cell-derived inducing activity. Neuron. Oct 2000;28(1):31-40.

8. Lee SH, Lumelsky N, Studer L, et al. Efficient generation of midbrain and hindbrain neurons from mouse embryonic stem cells. Nat Biotechnol. Jun 2000;18(6):675-679.

9. Bjorklund LM, Sanchez-Pernaute R, Chung S, et al. Embryonic stem cells develop into functional dopaminergic neurons after transplantation in a Parkinson rat model. Proc Natl Acad Sci U S A. Feb 19 2002;99(4):2344-2349.

10. Kim JH, Auerbach JM, Rodriguez-Gomez JA, et al. Dopamine neurons derived from embryonic stem cells function in an animal model of Parkinson's disease. Nature. Jul 4 2002;418(6893):50-56.

11. Barberi T, Klivenyi P, Calingasan NY, et al. Neural subtype specification of fertilization and nuclear transfer embryonic stem cells and application in parkinsonian mice. Nat Biotechnol. Oct 2003;21(10):1200-1207.

12. Takagi Y, Takahashi J, Saiki H, et al. Dopaminergic neurons generated from monkey embryonic stem cells function in a Parkinson primate model. J Clin Invest. Jan 2005;115(1):102-109.

13. Sanchez-Pernaute R, Studer L, Ferrari D, et al. Long-term survival of dopamine neurons derived from parthenogenetic primate embryonic stem cells (Cyno1) after transplantation. Stem Cells. Aug 2005;23(7):914-922.

14. Kim DW, Chung S, Hwang M, et al. Stromal cell-derived inducing activity, nurr1, and signaling molecules synergistically induce dopaminergic neurons from mouse embryonic stem cells. Stem Cells. Mar 2006;24(3):557-567.

15. Zeng X, Cai J, Chen J, et al. Dopaminergic differentiation of human embryonic stem cells. Stem Cells. 2004;22(6):925-940.

16. Ben-Hur T, Idelson M, Khaner H, et al. Transplantation of human embryonic stem cell-derived neural progenitors improves behavioral deficit in Parkinsonian rats. Stem Cells. 2004;22(7):1246-1255.

17. Park CH, Minn YK, Lee JY, et al. In vitro and in vivo analyses of human embryonic stem cell-derived dopamine neurons. J Neurochem. Mar 2005;92(5):1265-1276.

18. Yan Y, Yang D, Zarnowska ED, et al. Directed differentiation of dopaminergic neuronal subtypes from human embryonic stem cells. Stem Cells. Jun-Jul 2005;23(6):781-790.

19. Brederlau A, Correia AS, Anisimov SV, et al. Transplantation of human embryonic stem cell-derived cells to a rat model of Parkinson's disease: effect of in vitro differentiation on graft survival and teratoma formation. Stem Cells. Mar 23 2006.

20. Roy NS, Cleren C, Singh SK, Yang L, Beal MF, Goldman SA. Functional engraftment of human ES cell-derived dopaminergic neurons enriched by coculture with telomerase-immortalized midbrain astrocytes. Nat Med. Oct 22 2006.

21. Nikkhah G, Duan WM, Knappe U, Jodicke A, Bjorklund A. Restoration of complex sensorimotor behavior and skilled forelimb use by a modified nigral cell suspension transplantation approach in the rat Parkinson model. Neuroscience. Sep 1993;56(1):33-43.

22. Seidel J, Vaquero J, Green M. Resolution uniformity and sensitivity of the NIH ATLAS small animal PET scanner: comparison to simulated LSO scanners without depth-of-interaction capability. IEEE Trans Nucl Sci. 2003; 50:1347-1350.

23. Johnson CA, Seidel J, Vaquero JJ, et al. Exact positioning for OSEM reconstructions on the ATLAS depth-of-interaction small animal scanner. Mol Imaging Biol. 2002;4:S22.

24. Liow J, Seidel J, Johnson CA et al. A single slice rebinning/2D exact positioning OSEM reconstruction for the NIH ATLAS small animal PET scanner. J Nucl Med. 2003; 44:163P.

25. Ichise M, Liow JS, Lu JQ, et al. Linearized reference tissue parametric imaging methods: application to [^{11}C]DASB positron emission tomography studies of the

serotonin transporter in human brain. J Cereb Blood Flow Metab. Sep 2003;23(9):1096-1112.

26. Goodman MM, Kilts CD, Keil R, et al. ^{18}F-labeled FECNT: a selective radioligand for PET imaging of brain dopamine transporters. Nucl Med Biol. Jan 2000;27(1):1-12.

27. Davis MR, Votaw JR, Bremner JD, et al. Initial human PET imaging studies with the dopamine transporter ligand ^{18}F-FECNT. J Nucl Med. Jun 2003;44(6):855-861.

28. Zoghbi SS, Shetty HU, Ichise M, et al. PET Imaging of the Dopamine Transporter with ^{18}F-FECNT: A Polar Radiometabolite Confounds Brain Radioligand Measurements. J Nucl Med. Mar 2006;47(3):520-527.

29. Laruelle M, Abi-Dargham A, al-Tikriti MS, et al. SPECT quantification of [^{123}I]iomazenil binding to benzodiazepine receptors in nonhuman primates: II. Equilibrium analysis of constant infusion experiments and correlation with in vitro parameters. J Cereb Blood Flow Metab. May 1994;14(3):453-465.

30. Thanos PK, Taintor NB, Alexoff D, et al. In vivo comparative imaging of dopamine D2 knockout and wild-type mice with ^{11}C-raclopride and microPET. J Nucl Med. Nov 2002;43(11):1570-1577.

31. Alexoff DL, Vaska P, Marsteller D, et al. Reproducibility of ^{11}C-raclopride binding in the rat brain measured with the microPET R4: effects of scatter correction and tracer specific activity. J Nucl Med. May 2003;44(5):815-822.

32. Matej S, Karp JS, Lewitt RM, et al. Performance of the Fourier rebinning algorithm for PET with large acceptance angles. Phys Med Biol. Apr 1998;43(4):787-795.

33. Paxinos G, Watson C. The Rat Brain in Stereotaxic Coordinates, 4th ed. New York: Academic Press, 1998.

34. Lammertsma AA, Bench CJ, Hume SP, et al. Comparison of methods for analysis of clinical [^{11}C]raclopride studies. J Cereb Blood Flow Metab. Jan 1996;16(1):42-52.

35. Lassen NA. Neuroreceptor quantitation in vivo by the steady-state principle using constant infusion or bolus injection of radioactive tracers. J Cereb Blood Flow Metab. Sep 1992;12(5):709-716.

36. Ye W, Shimamura K, Rubenstein JL, et al. FGF and Shh signals control dopaminergic and serotonergic cell fate in the anterior neural plate. Cell. May 29 1998;93(5):755-766.

37. Simon HH, Saueressig H, Wurst W, et al. Fate of midbrain dopaminergic neurons controlled by the engrailed genes. J Neurosci. May 1 2001;21(9):3126-3134.

38. Smidt MP, Asbreuk CH, Cox JJ, et al. A second independent pathway for development of mesencephalic dopaminergic neurons requires Lmx1b. Nat Neurosci. Apr 2000;3(4):337-341.

39. Ruiz i Altaba A, Prezioso VR, Darnell JE, et al. Sequential expression of HNF-3 beta and HNF-3 alpha by embryonic organizing centers: the dorsal lip/node, notochord and floor plate. Mech Dev. Dec 1993;44(2-3):91-108.

40. Andersson E, Tryggvason U, Deng Q, et al. Identification of intrinsic determinants of midbrain dopamine neurons. Cell. Jan 27 2006;124(2):393-405.

41. Wolfrum C, Besser D, Luca E, et al. Insulin regulates the activity of forkhead transcription factor Hnf-3beta/Foxa-2 by Akt-mediated phosphorylation and nuclear/cytosolic localization. Proc Natl Acad Sci U S A. Sep 30 2003;100(20):11624-11629.

42. Smidt MP, van Schaick HS, Lanctot C, et al. A homeodomain gene Ptx3 has highly restricted brain expression in mesencephalic dopaminergic neurons. Proc Natl Acad Sci U S A. Nov 25 1997;94(24):13305-13310.

43. Gerfen CR, Herkenham M, Thibault J. The neostriatal mosaic: II. Patch- and matrix-directed mesostriatal dopaminergic and non-dopaminergic systems. J Neurosci. Dec 1987;7(12):3915-3934.

44. McCaffery P, Drager UC. High levels of a retinoic acid-generating dehydrogenase in the meso-telencephalic dopamine system. Proc Natl Acad Sci U S A. Aug 2 1994;91(16):7772-7776.

45. Chung S, Hedlund E, Hwang M, et al. The homeodomain transcription factor Pitx3 facilitates differentiation of mouse embryonic stem cells into AHD2-expressing dopaminergic neurons. Mol Cell Neurosci. Feb 2005;28(2):241-252.

46. Amara SG, Kuhar MJ. Neurotransmitter transporters: recent progress. Annu Rev Neurosci. 1993;16:73-93.

47. Giros B, Caron MG. Molecular characterization of the dopamine transporter. Trends Pharmacol Sci. Feb 1993;14(2):43-49.

48. Jellinger KA. The pathology of Parkinson's disease. Adv Neurol. 2001;86:55-72.

49. Takeuchi Y, Sawada T, Blunt S, Jenner P, Marsden CD. Serotonergic sprouting in the neostriatum after intrastriatal transplantation of fetal ventral mesencephalon. Brain Res. Jun 14 1991;551(1-2):171-177.

50. Wright AK, Arbuthnott GW, Dunnett SB. Serotonin hyperinnervation after foetal nigra or raphe transplantation in the neostriatum of adult rats. Neurosci Lett. Jul 22 1991;128(2):281-284.

51. Khoshbouei H, Sen N, Guptaroy B, et al. N-terminal phosphorylation of the dopamine transporter is required for amphetamine-induced efflux. PLoS Biol. Mar 2004;2(3):E78.

52. Zetterstrom T, Sharp T, Collin AK, et al. In vivo measurement of extracellular dopamine and DOPAC in rat striatum after various dopamine-releasing drugs; implications for the origin of extracellular DOPAC. Eur J Pharmacol. Apr 13 1988;148(3):327-334.

53. Brooks DJ, Frey KA, Marek KL, et al. Assessment of neuroimaging techniques as biomarkers of the progression of Parkinson's disease. Exp Neurol. Nov 2003;184 Suppl 1:S68-79.

54. Piccini P, Whone A. Functional brain imaging in the differential diagnosis of Parkinson's disease. Lancet Neurol. May 2004;3(5):284-290.

55. Piccini P, Brooks DJ, Bjorklund A, et al. Dopamine release from nigral transplants visualized in vivo in a Parkinson's patient. Nat Neurosci. Dec 1999;2(12):1137-1140.

56. Nakamura T, Dhawan V, Chaly T, et al. Blinded positron emission tomography study of dopamine cell implantation for Parkinson's disease. Ann Neurol. Aug 2001;50(2):181-187.

57. Bjorklund A, Dunnett SB, Brundin P, et al. Neural transplantation for the treatment of Parkinson's disease. Lancet Neurol. Jul 2003;2(7):437-445.

58. Hume SP, Opacka-Juffry J, Myers R, et al. Effect of L-dopa and 6-hydroxydopamine lesioning on [^{11}C]raclopride binding in rat striatum, quantified using PET. Synapse. Sep 1995;21(1):45-53.

59. Farooqui SM. Induction of adenylate cyclase sensitive dopamine D2-receptors in retinoic acid induced differentiated human neuroblastoma SHSY-5Y cells. Life Sci. 1994;55(24):1887-1893.

60. Samad TA, Krezel W, Chambon P, et al. Regulation of dopaminergic pathways by retinoids: activation of the D2 receptor promoter by members of the retinoic acid receptor-retinoid X receptor family. Proc Natl Acad Sci U S A. Dec 23 1997;94(26):14349-14354.

61. Valdenaire O, Maus-Moatti M, Vincent JD, et al. Retinoic acid regulates the developmental expression of dopamine D2 receptor in rat striatal primary cultures. J Neurochem. Sep 1998;71(3):929-936.

62. Krezel W, Ghyselinck N, Samad TA, et al. Impaired locomotion and dopamine signaling in retinoid receptor mutant mice. Science. Feb 6 1998;279(5352):863-867.

63. Dunnett SB, Hernandez TD, Summerfield A, et al. Graft-derived recovery from 6-OHDA lesions: specificity of ventral mesencephalic graft tissues. Exp Brain Res. 1988;71(2):411-424.

64. Zetterstrom T, Brundin P, Gage FH, et al. In vivo measurement of spontaneous release and metabolism of dopamine from intrastriatal nigral grafts using intracerebral dialysis. Brain Res. Jan 8 1986;362(2):344-349.

65. Strecker RE, Sharp T, Brundin P, et al. Autoregulation of dopamine release and metabolism by intrastriatal nigral grafts as revealed by intracerebral dialysis. Neuroscience. Jul 1987;22(1):169-178.

66. Rioux L, Gaudin DP, Bui LK, et al. Correlation of functional recovery after a 6-hydroxydopamine lesion with survival of grafted fetal neurons and release of dopamine in the striatum of the rat. Neuroscience. 1991;40(1):123-131.

67. Gnegy ME, Khoshbouei H, Berg KA, et al. Intracellular Ca2+ regulates amphetamine-induced dopamine efflux and currents mediated by the human dopamine transporter. Mol Pharmacol. Jul 2004;66(1):137-143.

68. Inaji M, Yoshizaki T, Okauchi T, et al. In vivo PET measurements with [^{11}C]PE2I to evaluate fetal mesencephalic transplantations to unilateral 6-OHDA-lesioned rats. Cell Transplant. 2005;14(9):655-663.

69. Freed WJ, Ko GN, Niehoff DL, et al. Normalization of spiroperidol binding in the denervated rat striatum by homologous grafts of substantia nigra. Science. 1983; 222: 937-939.

70. Dawson TM, Dawson VL, Gage FH, et al. Functional recovery of supersensitive dopamine receptors after intrastriatal grafts of fetal substantia nigra. Exp Neurol. Mar 1991;111(3):282-292.

71. Rioux L, Gaudin DP, Gagnon C, Di Paolo T, Bedard PJ. Decrease of behavioral and biochemical denervation supersensitivity of rat striatum by nigral transplants. Neuroscience. 1991;44(1):75-83.

72. Kalen P, Nilsson OG, Cenci MA, et al. Intracerebral microdialysis as a tool to monitor transmitter release from grafted cholinergic and monoaminergic neurons. J Neurosci Methods. Sep 1990;34(1-3):107-115.

73. Wang Y, Wang SD, Lin SZ, et al. Restoration of dopamine overflow and clearance from the 6-hydroxydopamine lesioned rat striatum reinnervated by fetal mesencephalic grafts. J Pharmacol Exp Ther. Aug 1994;270(2):814-821.

74. Stromberg I, van Horne C, Bygdeman M, et al. Function of intraventricular human mesencephalic xenografts in immunosuppressed rats: an electrophysiological and neurochemical analysis. Exp Neurol. May 1991;112(2):140-152.

75. Cragg SJ, Clarke DJ, Greenfield SA. Real-time dynamics of dopamine released from neuronal transplants in experimental Parkinson's disease. Exp Neurol. Jul 2000;164(1):145-153.

76. Stromberg I, Kehr J, Andbjer B, et al. Fetal ventral mesencephalic grafts functionally reduce the dopamine D2 receptor supersensitivity in partially dopamine reinnervated host striatum. Exp Neurol. Jul 2000;164(1):154-165.

77. Day M, Wang Z, Ding J, et al. Selective elimination of glutamatergic synapses on striatopallidal neurons in Parkinson disease models. Nat Neurosci. Feb 2006;9(2):251-259.

Table 1. Basal levels of monoamines (nM) in perfusates from striatum of sham and grafted animals in lesioned and non-lesioned sides.

Treatment	**Sham**		**Grafted**	
Side	**Left lesioned**	**Right non-lesioned**	**Left lesioned**	**Right non-lesioned**
DA	0.76 ± 0.10	0.78 ± 0.06	2.18 ± 0.16 [a]	2.05 ± 0.69
DOPAC	4.26 ± 2.07 [b]	3105 ± 707	233 ± 44 [a]	2861 ± 734
HVA	3.87 ± 2.53 [b]	2283 ± 437	240 ± 41 [a]	2110 ± 421
5-HIAA	115 ± 35	127 ± 38	362 ± 78 [a]	204 ± 55

Table 1. Data (mean ± S.E.M.) are averaged from three baseline samples (paired *t*-test; [a] $p < 0.01$ left grafted vs. left and right sham sides; [b] $p < 0,01$ left sham vs. right sham).

Figure legends:

Figure 1. Expression pattern of midbrain related markers by progenitors and differentiated neurons generated from ES cells. **A)** Triple immunocytochemical labelling for En1, Lmx1b and Foxa2 in progenitor cells (day 4, stage 4). **B)** Different cell populations expressing different combinations of genes were observed at this stage. The results are shown as mean ± S.E.M. **C)** Triple immunocytochemical labelling in differentiated DA neurons (day 10, stage 5). TH+ cells express neuronal marker Hu. Foxa2 expression is maintained in differentiated TH+ neurons. En1 is expressed in TH+ neurons and Ptx3 expression emerges in most of them. Few TH+ neurons expressed calbindin, which did not co-localized with Ptx3 gene. A fraction of TH+ neurons (42 ± 1 %) expressed RALDH1 protein. Some TH+ also co-expressed DAT. Scale = 20 μm.

Figure 2. Behavioral recovery after ES cell-derived DA neuron grafting, phenotype of grafted DA neurons and restoration of DA terminal field in 6-OHDA lesioned striatum by grafted cells. **A)** Grafting of ES cells caused significant recovery of amphetamine-induced rotational behavior. The results are shown as mean ± S.E.M. (n = 5; *, $P<0.01$; $^{\#}$, $P < 0.05$ by a two-tailed *t*-test, compared with rats receiving sham treatment). **B)** Double immunocytochemical staining of grafted DA neurons performed at the endpoint of the experiment, i.e. 32 weeks after transplantation. Donor origin of grafted DA neurons was confirmed by co-labelling with the mouse-specific antigen M2. Some TH+ neurons co-expressed RALDH1 and we also found TH+/calbindin+ neurons. Double positive neurons for TH and calretinin were present, as well as TH-/calretinin+ cells. Scale = 20 μm. **C**) ES cell-derived DA neurons partially restored TH and RALDH1 immunoreactivity in the lesioned side. TH (green) immunostaining is shown for the grafted (left, $\mathbf{C_1}$) and non-lesioned (right, $\mathbf{C_2}$) sides and RALDH1 (red) is shown for the

grafted ($\mathbf{C_3}$) and non-lesioned ($\mathbf{C_4}$) sides. DAPI staining is shown in blue color. Scale = 1 mm.

Figure 3. Effect of ES cell-derived DA neuron graft on monoamine levels studied *in vivo* by microdialysis performed 12 weeks after grafting. **A)** Time-course on DA concentration level after 100 mM K+ isosmotic medium, 50 μM nomifensine and 30 μM amphetamine in the lesioned and non-lesioned sides of sham and grafted animals. **B)** Time-course on DA level shown in **A** for lesioned sides in grafted and sham groups is shown at bigger scale. **C)** Time-course of DOPAC and HVA concentrations for non-lesioned sides of both sham and grafted animals and for the lesioned side that received DA neurons. The results are shown as mean ± S.E.M. (n = 5; *, $P<0.01$; $^{\#}$, $P < 0.05$ by a two-tailed *t*-test, compared with rats receiving the sham treatment).

Figure 4. Dynamic PET imaging in naïve rats with [^{18}F]FECNT. **A)** About 30 min after bolus injection of [^{18}F]FECNT (n = 5), activity in cerebellum (CBL) was stable despite declining concentrations in striatum (STR). **B)** After ~150 min of constant infusion of [^{18}F]FECNT (n = 5), activities in striatum and cerebellum increased in a linear and parallel manner. Specific binding (SPEC) was operationally defined as the difference between striatum and cerebellum and, therefore, became stable after ~150 min. The plasma concentration of [^{18}F]FECNT separated from radiometabolites (upper curve) after ~170 min of infusion was also obtained. The *y*-axis on left is for brain measurements and is expressed as % of the activity infused per h. The *y*-axis on right is the plasma measurements of the concentration of [^{18}F]FECNT and is expressed as a percentage of the constant infusion: [(plasma [^{18}F]FECNT dpm/mL)/ activity (mCi) infused per hour] * 100. **C)** The difference in TACs between striatum and cerebellum

was confirmed to be specific binding, since methylphenidate displaced [^{18}F]FECNT in striatum to background levels in cerebellum (n = 4).

Figure 5. Recovery on DAT binding after grafting of 6-OHDA lesioned animals performed 24-28 weeks after transplantation. **A)** A naïve rat showed bilaterally symmetrical uptake of [^{18}F]FECNT in striata following constant infusion of the radiotracer. **B)** A hemiparkinsonian rat receiving sham treatment displayed negligible uptake in the lesioned striatum**. C)** ES-cell transplantation partially restored uptake of [^{18}F]FECNT in the lesioned striatum of a hemiparkinsonian rat. **D)** PET and MRI images of hemiparkinsonian rat with ES-cell transplantation into the left striatum were coregistered to define anatomic structures. **E)** ES-cell transplantation increased the ratio of activity in lesioned/non-lesioned striatum determined by PET imaging with [^{18}F]FECNT. The ratio was greatly reduced in hemiparkinsonian rats that had either no intervention (n = 4) or sham treatment (n = 5). This reduced ratio significantly recovered after transplanting ES-cells into the lesioned striatum of hemiparkinsonian rats (n = 5; *, $p < 0.01$ by a two-tailed *t*-test, compared with rats receiving the sham treatment). The horizontal line on each group shows the mean value.

Figure 6. Recovery on [^{18}F]FECNT specific binding after grafting of 6-OHDA lesioned animals. Time activity curves following constant infusion of [^{18}F]FECNT in rats with (**A**) sham treatment and (**B**) ES cell transplantation. After 120-150 min constant infusion, uptake in both striatum (STR) and cerebellum (CBL) ascended linearly, and specific binding (SPEC = STR - CBL) became stable. Specific binding in the lesioned striatum displayed a minimal level in rats receiving sham treatment (**A**; n = 5), but increased to approximately 1/3 level of non-lesioned striatum after ES cell

transplantation (**B**; n = 5). The *y*-axis is expressed as % of the activity infused per h. Results are shown as mean ± S.E.M. **C)** Distribution volumes of [^{18}F]FECNT specific binding in striata of hemiparkinsonian rats. The distribution volumes of the non-lesioned striata were similar in sham (n = 5) and ES cell transplanted (n = 5) animals. In contrast, the distribution volumes of the lesioned striata were significantly higher in transplanted than in sham animals (6.71 ± 1.7 vs. 1.15 ± 0.23; *, $p < 0.01$ by a two-tailed *t*-test, compared with rats receiving the sham treatment). The horizontal line on each group shows the mean value.

Supplementary figure legend:

Figure S1. Non-pharmacological evaluation of rotational behavior demonstrates significant recovery 14 weeks after transplantation. The results are shown as mean ± S.E.M. (n = 5; *, P<0.05 by a two-tailed *t*-test, compared with rats receiving sham treatment).

Figure S2. Binding potential of [^{11}C]raclopride in striata of hemiparkinsonian rats measured by PET D_2 receptor scanning performed 32 weeks after transplantation. The lesioned striata of sham rats (n = 4) showed a significant increase in dopamine D_2 receptor binding compared to the contralateral, non-lesioned side ($p < 0.01$, paired two-tailed *t*-test). In contrast, receptor binding in transplanted animals (n = 5) was equal on right and left sides and significantly different from left side of sham animals (p=0.01). Results are shown as mean ± S.E.M.

Figure 1

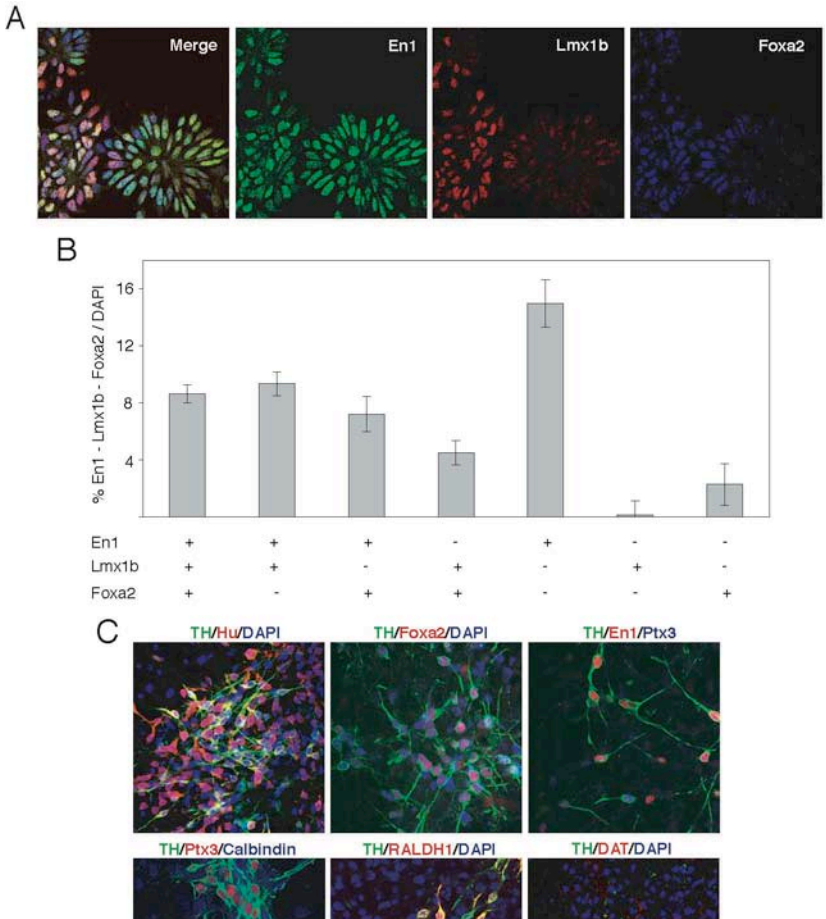

Figure 2

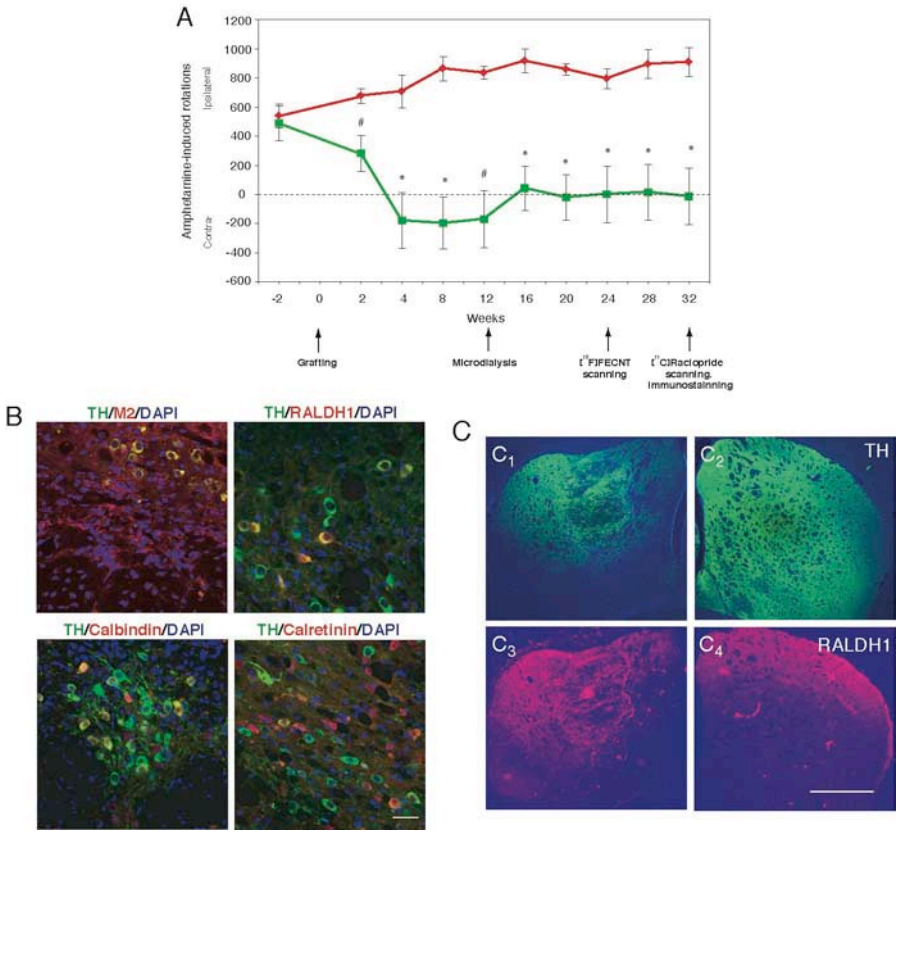

Figure 3

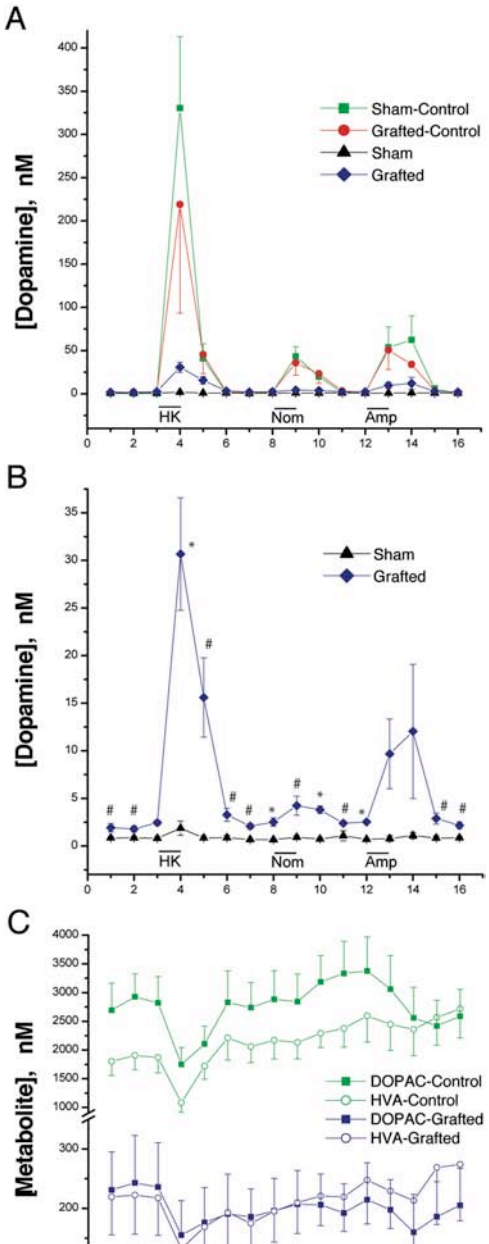

Figure 4

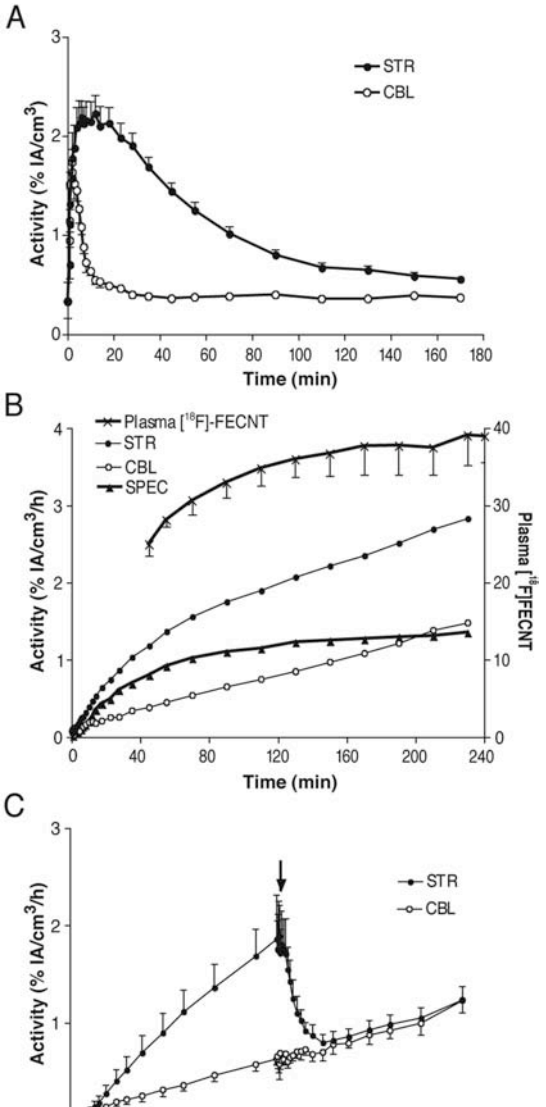

Figure 5

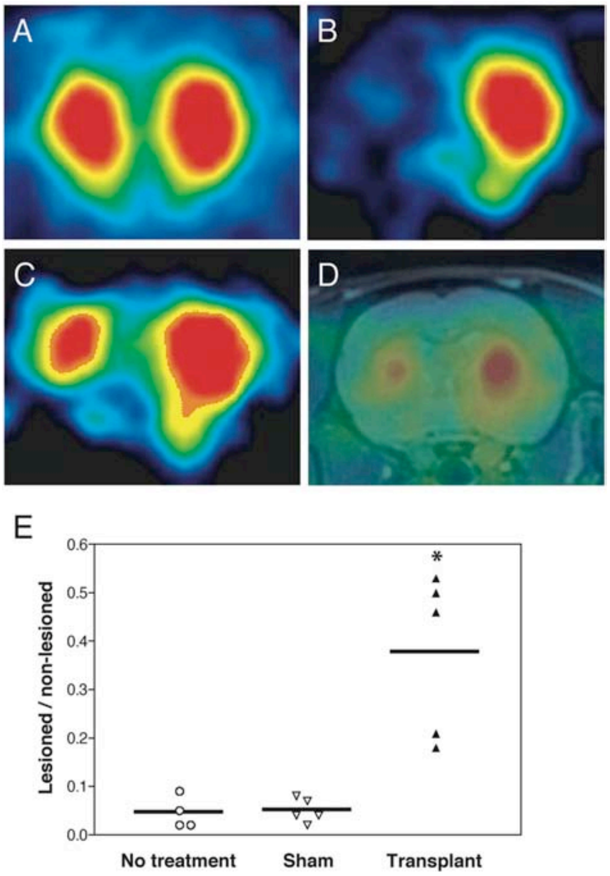

Figure 6

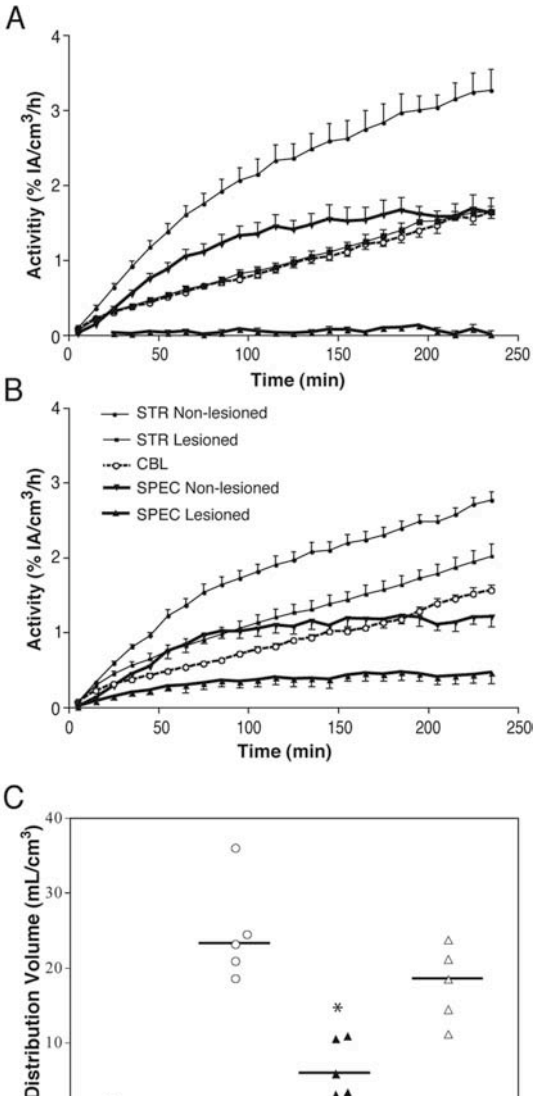

Supplemental Figure 1

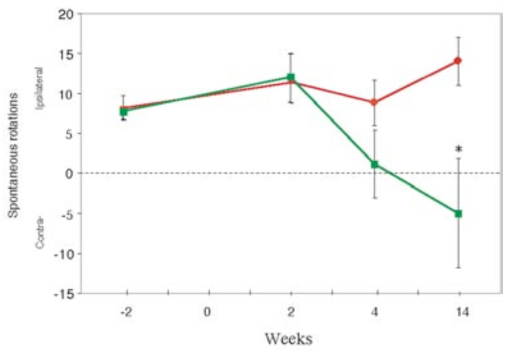

Supplemental Figure 2

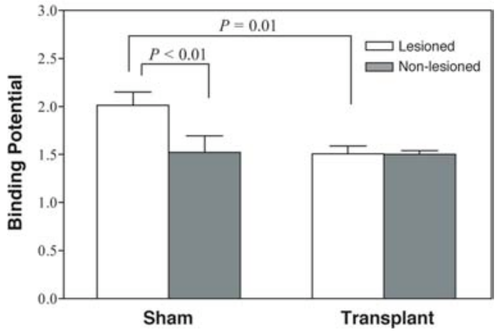

Persistent dopamine functions of neurons derived from embryonic stem cells in a rodent model of Parkinson's disease

Jose A. Rodríguez-Gómez, Jian-Qiang Lu, Iván Velasco, Seth Rivera, Sami S. Zoghbi, Jeih-San Liow, John L. Musachio, Frederick T. Chin, Hiroshi Toyama, Jurgen Seidel, Michael V. Green, Panayotis K. Thanos, Masanori Ichise, Victor W. Pike, Robert B. Innis and Ron D.G. McKay

Stem Cells published online Dec 14, 2006;
DOI: 10.1634/stemcells.2006-0386